Hanbury Brown and Twiss exchange correlations in a graphene box

Teemu Elo,[1,*] Zhenbing Tan,[1,†] Ciprian Padurariu,[1,2] Fabian Duerr,[3] Dmitry S. Golubev,[1,‡] Gordey B. Lesovik,[4] and Pertti Hakonen[1,§]

[1]*Low Temperature Laboratory, Department of Applied Physics, Aalto University, Espoo, Finland*
[2]*Institute for Complex Quantum Systems and IQST, Ulm University, Ulm, Germany*
[3]*Physikalisches Institut (EP3), University of Würzburg, Würzburg, Germany*
[4]*Moscow Institute of Physics and Technology, Moscow 141700, Russian Federation*

(Received 12 September 2019; published 18 December 2019)

Quadratic detection in linear mesoscopic transport systems produces cross terms that can be viewed as interference signals reflecting statistical properties of charge carriers. In electronic systems these cross-term interferences arise from exchange effects due to Pauli principle. Here we demonstrate fermionic Hanbury Brown and Twiss (HBT) exchange phenomena due to indistinguishability of charge carriers in a diffusive graphene system. These exchange effects are verified using current-current cross-correlations in combination with regular shot noise (autocorrelation) experiments at microwave frequencies. Our results can be modeled using semiclassical analysis for a square-shaped metallic diffusive conductor, including contributions from contact transparency. The experimentally determined HBT exchange factor values lie between the calculated ones for coherent and hot electron transport.

DOI: 10.1103/PhysRevB.100.235433

I. INTRODUCTION

Shot noise is a widely used characterization method in nanophysics, as it can provide more information on the charge transport than conventional conductance or thermal noise measurements [1–4]. Multiterminal current-current correlation experiments provide additional insight into intrinsic characteristics of charge carriers in mesoscopic systems. For example, they allow one to distinguish bosonic and fermionic carriers [5–7].

Many of the noise and cross-correlation experiments probing fundamental properties of the charge carriers have been performed using edge states in the quantum Hall regime, in which quantum point contacts with tunable transparency control the propagation of coherent beams of electrons or composite fermions [8]. In this setup, one can perform two-particle scattering experiments and observe Hanbury Brown and Twiss [9] (HBT) interference effects in current-current cross-correlation [10], which are not visible in Aharonov-Bohm conductance experiments. In a regular mesoscopic conductor the phase-dependent phenomena in two-particle scattering events are averaged out over many possible trajectories [11]. However, even after such averaging current-current cross-correlations in different terminals are affected by Fermi statistics of electrons in a nontrivial way. One well-known consequence of Fermi statistics is the negative sign of cross-correlations between the currents in different terminals [2]. In this work we investigate another interesting consequence—the nonadditive nature of cross-correlations [11,12]—in a HBT setup [9,10] with two sources and two detectors attached to a diffusive graphene flake. Below we will refer to the nonadditivity of the noise cross-correlations as HBT exchange effect.

To our knowledge, only one experiment has so far addressed HBT exchange effects in diffusive conductors. Cross-correlations and HBT exchange were measured in a cross-shaped graphene conductor in which the charge carrier density, and thereby the screening of impurities, could be tuned by the back gate voltage [13]. According to the theory, in a diffusive conductor with cross geometry the paths of scattering electrons are quite restricted, and the HBT exchange effect should disappear [11,12]. However, the experiment showed a finite exchange effect, which was attributed to an appreciable mean-free path of electrons, comparable to the size of the crossing.

In charge neutral graphene, ideally, electrical transport takes place via evanescent waves, the distribution of which mimics diffusive electron transport [14–17]. Since the evanescent waves may propagate to both measuring terminals, special cross-correlations are obtained in graphene near the charge neutrality point (CNP) [18]. According to the tight-binding calculations of Ref. [18], there is a negative HBT exchange effect at the Dirac point. Instead of diffusive-like shot noise due to evanescent waves, experiments have shown more complex behavior in graphene [19–21]. For graphene ribbons, Coulomb blockade effects and localization have been found to influence the shot noise results substantially [22]. Therefore, also shot noise cross-correlations can be expected to differ from those appearing in pure diffusive transport and to exhibit features inherent to disordered graphene samples.

*teemu.elo@aalto.fi
†Present address: Shenzhen Institute for Quantum Science and Engineering, and Department of Physics, Southern University of Science and Technology, Shenzhen 518055, China.
‡Present address: QTF Centre of Excellence, Department of Applied Physics, Aalto University, FI-00076 Aalto, Finland.
§pertti.hakonen@aalto.fi

In this work we study the HBT exchange effect in a coherent square-shaped graphene conductor with a short mean-free path and diffusive transport of electrons. We measure both current-current cross-correlations at microwave frequencies and regular shot noise of the contacts (autocorrelation). We model our results using semiclassical analysis for a diffusive coherent conductor, in which the noise arises locally due to the nonequilibrium distribution of electrons. We repeat the analysis in the hot electron regime, where the noise is characterized by local temperature distribution. The best agreement between experiment and theory is obtained in the crossover regime between the coherent and hot electron models.

This article is organized as follows. We start with the theoretical background (Sec. II), and outline the basics of shot noise, cross-correlations, and the Hanbury Brown and Twiss exchange effect in fermionic systems. In Sec. II A, we describe briefly the semiclassical analysis and present our models for coherent and hot electron regimes. The parameters for the numerical noise calculations are obtained from the conductance distribution of our sample, analyzed in Sec. II B, while the noise calculations are presented in Sec. II C. Our experimental methods are concisely covered in Sec. III, while results are presented in Sec. IV. The discussion in Sec. V includes connections of our work to other noise experiments and discusses a few theoretical issues relevant for the bias and gate voltage dependence of our data. Section VI concludes the paper.

II. THEORETICAL BACKGROUND

A random flow of electrons with charge e can be described as an uncorrelated Poisson process [23], which gives rise to the spectral density of the shot noise, $S_I = 2eI$, where I is the current through the conductor. In contrast to thermal fluctuations in mesoscopic conductors, shot noise provides information on the basic transport properties beyond the linear response theory coefficients such as conductance. In mesoscopic systems, shot noise can become sub-Poissonian under the influence of interactions or correlations, for example, imposed by the Pauli principle [24–28]. The ensuing noise spectral density can be written as $S_I = F2eI$, where F denotes the so called Fano factor. In a tunnel junction with low transmission, $F = 1$ because electron tunneling in such a junction is a Poissonian process [2]. In a ballistic conductor the shot noise is fully suppressed, while suppression down to $F = 1/3$ is found in diffusive conductors [2,29,30].

The Pauli principle also influences the cross-correlations of current fluctuations in a diffusive system. The cross-correlation of the fluctuations of the currents entering the conductor through terminals m and n, S_{nm}, is defined by

$$S_{nm} = \int_{-\infty}^{\infty} dt \, \langle \delta\tilde{I}_n(t)\delta\tilde{I}_m(0)\rangle, \tag{1}$$

where we assume the low-frequency limit $eV \gg \hbar\omega$ relevant to our experiments. Our sample, shown in Fig. 1(a), has four terminals, which are the metallic leads attached to the corners of the box.

One can derive a very general expression [2] for the cross-correlation [Eq. (1)] in terms of the scattering matrix of the device $\hat{s}_{mn}$. For practical calculations we use an alternative approach based on the solution of the Boltzmann-Langevin equation for diffusive electrons inside the box [11,12], which we outline in the next subsection. The two approaches are equivalent because the scattering matrix can be expressed in terms of the electronic retarded (G^R) and advanced (G^A) Green's functions and transmission probabilities of the conducting channels of the terminals [31]. Performing disorder averaging of the products $G^R G^A$ in the diffusive conductor with the aid of the standard rules [32], one can reduce the evaluation of the cross-correlations [Eq. (1)] to the solution of the diffusion equation.

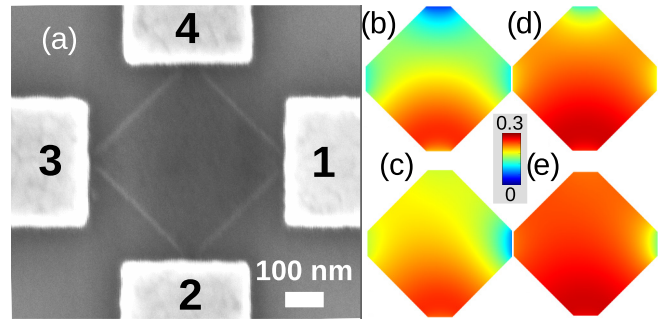

FIG. 1. (a) Graphene box sample with Cr/Au contacts at the corners. The scale bar indicates 100 nm. The graphene extends under each contact by approximately 1 μm. Biasing is applied via ports 2 and 4, while cross-correlation S_{13} is measured between terminals 1 and 3. S_{13} is measured in three DC biasing situations: (A) $V_2 = V$ and $V_1 = V_3 = V_4 = 0$, (B) $V_4 = V$ and $V_1 = V_2 = V_3 = 0$, and (C) $V_2 = V_4 = V$ and $V_1 = V_3 = 0$, the results of which are marked by $-S_A$, $-S_B$, and $-S_C$, respectively. The Hanbury Brown and Twiss exchange effect is observed in the difference $\Delta S = S_C - S_A - S_B$. (b), (c) Nonequilibrium distribution functions in coherent regime described by Π [see Eq. (6)] for our diffusive graphene box that is biased from terminal 2 while the three other terminals are grounded at two gate voltage values: far from the charge neutrality point (CNP) ($V_g = -10$ V) (b) and near it ($V_g = +15$ V) (c). (d), (e) Equivalent temperature distribution in the hot electron regime [see Eq. (14)] in the same bias configuration as at $V_g = -10$ V (d) and $V_g = +15$ V (e). The color scale is relative to the applied bias voltage V.

Here our main focus is the HBT exchange effect which is probed by measuring the cross-correlation of the currents in terminals 1 and 3, denoted by S_{13}. The correlations are measured in three DC biasing configurations, namely A, B, and C. In the A (B) configuration terminal 2 (4) is biased with voltage V while the other three terminals are grounded. In the C configuration both terminals 2 and 4 are biased, while 1 and 3 are grounded. The measured current-current cross-correlations S_{13} are negative, but we follow the notation $S = -S_{13}$ used in Ref. [2] which has a positive sign. Finally, we consider the difference

$$\Delta S = S_C - S_A - S_B. \tag{2}$$

By obtaining the exchange correction factor ΔS from the measured electronic shot noise, our measurement essentially repeats the original HBT experiment performed with photons [9]. For distinguishable noninteracting particles the noises coming from different sources are additive and the combination [Eq. (2)] equals zero ($\Delta S = 0$). However, since the electrons are indistinguishable and obey Fermi statistics

one finds that $\Delta S \neq 0$. In theory the cross-correlation S_{13} is given by the sum of partial contributions $S_{13}^{\alpha\beta}$ containing the combinations of the distribution functions in the leads of the form $f_\alpha(1-f_\beta)+(1-f_\alpha)f_\beta$, $S_{13}=\sum_{\alpha,\beta=1}^{4} S_{13}^{\alpha\beta}$. The nonzero HBT exchange correction in Eq. (2) originates from the contribution S_{13}^{24} having the form [11]

$$S_{13}^{24} = \frac{2e^2}{\pi\hbar}\int dE\,\mathrm{Re}(\mathrm{Tr}[\hat{s}_{41}^{\dagger}\hat{s}_{12}\hat{s}_{23}^{\dagger}\hat{s}_{34}]) \times[(1-f_2)f_4+f_2(1-f_4)]. \tag{3}$$

Bias configurations A and B produce the same value for S_{13}^{24}, while it vanishes in the bias configuration C and at zero temperature due to the Pauli principle. Indeed, in this case one finds $(1-f_2)f_4+f_2(1-f_4)=0$ since $f_2=f_4=\theta(eV-E)$, where $\theta(x)$ is the Heaviside step function. Thus, at zero temperature one obtains [11]

$$\Delta S = 2S_{A,13}^{24} = \frac{4e^2}{\pi\hbar}\langle \mathrm{Re}(\mathrm{Tr}[\hat{s}_{41}^{\dagger}\hat{s}_{12}\hat{s}_{23}^{\dagger}\hat{s}_{34}])\rangle eV. \tag{4}$$

Here the angular brackets denote averaging over disorder in the diffusive conductor. The HBT exchange correction [Eqs. (2) and (4)] can be either positive or negative depending on the system parameters.

As we have mentioned earlier, after disorder averaging quantum interference effects vanish from the HBT exchange noise [Eq. (4)]. However, from a mathematical point of view one can still consider it as a classical interference effect for the distribution function of electrons. Indeed, the distribution function inside the graphene box f_0 is the linear combination of the distribution functions in the terminals, see Eq. (5), while the noise cross-correlation is the quadratic function of it. It is well known that the original HBT experiment [9] can also be interpreted in terms of the interference of classical waves. The interpretation of our experiment as an analogy to optical interference is discussed further in Sec. VI.

A. Semiclassical analysis

The nonequilibrium electron transport can be described by the Boltzmann-Langevin approach [12,33], which provides a simple and transparent interpretation of the theory. In this section we provide a brief summary of this approach and derive explicit expressions for the noise cross-correlations in terms of measurable parameters. We account for the effect of finite contact resistances and consider the two regimes: the regime of the elastic transport and the hot electron regime, in which electron-electron interaction leads to thermalization of the electrons and a local electronic temperature can be defined.

Considering the elastic transport regime, in which the electron-electron Coulomb interaction can be ignored, one obtains the solution of the Boltzmann equation for the electron distribution function in the form

$$f_0(\varepsilon,\boldsymbol{r}) = \sum_n \phi_n(\boldsymbol{r}) f_T(\varepsilon - eV_n), \tag{5}$$

where $\phi_n(\boldsymbol{r})$ denotes the potential distribution in a diffusive multiterminal conductor corresponding to the bias condition $V_m=\delta_{mn}$.

The noise correlations can be expressed in terms of a function Π which describes the nonequilibrium state of the biased multiterminal conductor:

$$\Pi(\boldsymbol{r}) = 2\int d\varepsilon\, f_0(\varepsilon - eV_k,\boldsymbol{r})[1-f_0(\varepsilon-eV_l,\boldsymbol{r})]. \tag{6}$$

If only one terminal is biased, the function simplifies to $\Pi = e\phi_k(1-\phi_k)|V|$ in the limit $T\to 0$. With two bias voltages, for example at terminals 2 and 4, one obtains $\Pi = e(\phi_2+\phi_4)[1-(\phi_2+\phi_4)]|V|$. Note that the nonlinear dependence of the distribution function (f_0) is carried over to dependence on the characteristic function (Π). Figures 1(b) and 1(c) display the numerically calculated Π functions for a graphene box where the contacts are placed in the corners of the box and their effective width is taken as 20% of the side length L. The shape of the Π function characterizes the diffusion of electrons governed by quantum statistics of fermions.

The noise currents in each terminal can be obtained by integrating the Π function. For example, the expression for the noise cross-correlations in a graphene box with perfect contacts reads

$$S_{ij} = \frac{1}{R_\square}\int d^2\boldsymbol{r}\,\Pi(\boldsymbol{r})\nabla\phi_i(\boldsymbol{r})\nabla\phi_j(\boldsymbol{r}), \tag{7}$$

where $R_\square$ is the sheet resistance of graphene. In our experimental configuration with finite contact resistances $\phi_n(\boldsymbol{r})$ exhibit jumps across the contacts, which reflect finite voltage drops on them. The effect of the contacts on the noise cross-correlations is discussed below.

One can use the elastic approximation for the electron transport if the escape time of an electron out of the graphene quantum dot, τ_{esc}, is much shorter than the electron-electron energy relaxation time τ_{ee}, i.e., if $\tau_{\mathrm{esc}} \ll \tau_{\mathrm{ee}}$. In the opposite case, $\tau_{\mathrm{esc}} \gg \tau_{\mathrm{ee}}$, the hot electron regime becomes relevant. The time τ_{esc} is given by the expression

$$\frac{1}{\tau_{\mathrm{esc}}} = \frac{\delta_{\mathrm{d}}}{4\pi\hbar}\left(\frac{R_q}{R_\square}+\sum_{k=1}^{4}\frac{R_q}{R_k}\right), \tag{8}$$

where $R_q=h/e^2$ is the resistance quantum, R_k are the contact resistances, and δ_d is the level spacing in the square graphene dot,

$$\delta_d = \frac{\pi\hbar v_0}{L^2 k_{\mathrm{F}}}. \tag{9}$$

Here $v_0\approx 10^6$ m/s is the speed of electrons in graphene and k_{F} is the Fermi wave vector. The electron-electron relaxation time is estimated as [34],

$$\frac{1}{\tau_{\mathrm{ee}}} = \frac{2R_\square}{R_q}\frac{k_B T_e}{\hbar}\ln\left[\frac{R_q^3}{64R_\square^3}\frac{e^4 k_{\mathrm{F}}}{\hbar v_0 k_B T_e}\right], \tag{10}$$

where T_e is the average effective temperature of electrons inside the graphene box. The temperature T_e equals the bath temperature at low bias voltages applied to the contacts and may grow to higher values $T_e\sim eV$ in the hot electron regime. For the parameters of our sample listed in Table I we find that the times [Eqs. (8) and (10)] weakly depend on the gate voltage. The escape time approximately takes the value $\tau_{\mathrm{esc}}\approx 1$ ps, while the electron-electron relaxation time

TABLE I. Contact resistances (R_i) and graphene sheet resistivity ($R_\square$) used in the numerical calculations far from CNP ($V_g = -10$ V) and near it ($V_g = +15$ V).

V_g (V)	R_1 (kΩ)	R_2 (kΩ)	R_3 (kΩ)	R_4 (kΩ)	$R_\square$ (kΩ)
−10	1.39	1.50	1.66	5.38	1.65
+15	1.59	4.47	8.00	36.4	3.70

[Eq. (10)] may change from $\tau_{ee} \sim 50$ ps at the bath temperature $T_e = 20$ mK to much shorter values $\tau_{ee} \ll \tau_{esc}$ at high bias. Thus we expect our sample to be in an intermediate regime between ballistic and hot electron transport.

In presence of the inelastic electron-electron scattering the shape of the Π function changes. The kinetic equation for the distribution function can be relatively easily found in the hot electron regime $\tau_{ee} \ll \tau_{esc} \ll \tau_{e-ph}$, where τ_{e-ph} is the electron-phonon relaxation time. In this regime the electron distribution function has the equilibrium Fermi-Dirac form with coordinate-dependent electron temperature, which differs from the temperature of the substrate.

The function Π [Eq. (6)] can be expressed in terms of the characteristic functions $\phi_j(\boldsymbol{r})$ both in the elastic and the hot electron regimes. Performing this analysis and generalizing the expression [Eq. (7)] to the case of finite contact resistances, we derive explicit expressions for the cross-correlation of the noises in terms of the experimentally measurable parameters. Assuming that the electron transport is fully elastic and considering the low-temperature (or high-bias) limit $k_B T_0 \ll eV$ relevant to our experiment, we find

$$S_{ij} = \sum_{k=1}^{4} G_{ik} G_{jk} R_k^2 \mathcal{S}_k + \sum_{k,l=1}^{4} \frac{e|V_k - V_l|}{R_\square} \int d^2\boldsymbol{r}\, \phi_k(\boldsymbol{r})\phi_l(\boldsymbol{r}) \nabla\phi_i(\boldsymbol{r}) \nabla\phi_j(\boldsymbol{r}). \quad (11)$$

Here G_{ik} are the elements of the conductance matrix, which describe the combined effect of all contact resistances and the inner part of the graphene box, R_k are contact resistances, and $\mathcal{S}_k$ are the local noise sources of the contacts evaluated under the assumption of fixed potential of the graphene box. The latter have the form

$$\mathcal{S}_k = -e \sum_{l=1}^{4} G_{kl} |V_k - V_l| + \frac{e(1-F_k)R_k}{2} \sum_{p,l=1}^{4} G_{kl} G_{kp} |V_p - V_l|. \quad (12)$$

Here F_k is the Fano factor of the kth contact. The integral in the last term of Eq. (11) runs over the inner part of the graphene box excluding the corner areas, to which the metallic leads are attached.

In the hot electron regime and for $k_B T_0 \ll eV$ the cross-correlation takes the form

$$S_{ij} = \sum_{k=1}^{4} G_{ik} G_{jk} R_k^2 \mathcal{S}_k + \frac{2}{R_\square} \int d^2\boldsymbol{r}\, T_e(\boldsymbol{r}) \nabla\phi_i(\boldsymbol{r}) \nabla\phi_j(\boldsymbol{r}). \quad (13)$$

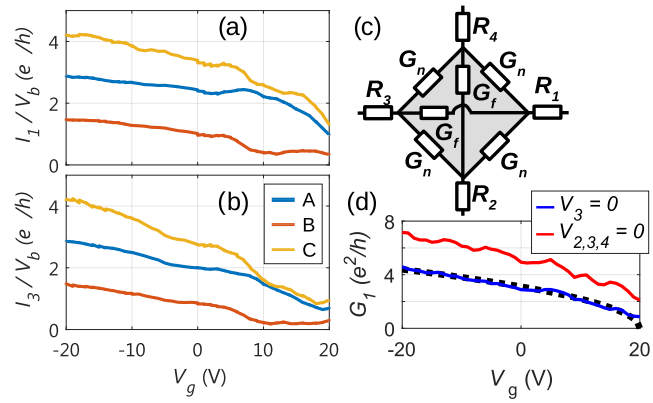

FIG. 2. (a), (b) Ratio of measured current and bias voltage at contacts 1 (a) and 3 (b) in bias configurations *A*, *B*, and *C*. (c) Schematic illustrating the division of the system into contacts and uniformly conducting graphene. The geometry used in our diffusive model yields $G_n = 1.6\, G_f$ and $R_\square = 0.165\, G_f^{-1}$. (d) Measured conductance as a function of gate voltage at contact 1 ($G_1 = I_1/V_1$) with other contacts grounded (red curve) and with contact 3 grounded and the other two floating ($I_2 = I_4 = 0$, blue curve). The dotted black line shows the fit to theoretical conductance of two constrictions [Eq. (17)] and the central region (with $R_1 + R_3 = 0.5 R_{tot}$) in series with $W = 50$ nm, $c_0 = 0.90$, and k_F set to its theoretical value ($V_{g,CNP}$ set to +20 V).

Here $T_e(\boldsymbol{r})$ is the coordinate-dependent electronic temperature inside the graphene box given by the expression

$$T_e(\boldsymbol{r}) = \sqrt{\frac{3e^2}{2\pi^2} \sum_{p,l=1}^{4} \phi_p(\boldsymbol{r})\phi_l(\boldsymbol{r})(V_p - V_l)^2}, \quad (14)$$

$\mathcal{S}_k$ are again the local junction noise sources, which now take the form

$$\mathcal{S}_k = \frac{F_k T_k}{R_k} \ln\left[2 + 2\cosh\left(\frac{eR_k \sum_{l=1}^{4} G_{kl}|V_k - V_l|}{T_k}\right)\right] + \frac{(1-F_k)T_k}{R_k}, \quad (15)$$

and T_k are the electronic temperatures inside the box close to the contacts,

$$T_k = \frac{\sqrt{3}eR_k}{\sqrt{2}\pi} \times \sqrt{\sum_{p,l=1}^{4} G_{kp}G_{kl}(V_k - V_l)^2 - \sum_{l=1}^{4} \frac{2G_{kl}}{R_k}(V_k - V_l)^2}. \quad (16)$$

B. Conductance

As described above, the conductances of graphene and contacts are parameters in our numerical noise model. Therefore, we use the measured conductances shown in Figs. 2(a), 2(b), and 2(d) as a starting point for the numerical noise calculations.

The measured conductances are used to construct a 4×4 conductance matrix for the whole system ($\mathbf{G}$) which is then divided into the central graphene part ($\tilde{\mathbf{G}}$) with uniform

conductivity and contact resistances (diagonal matrix $\mathbf{R}$), satisfying $\mathbf{G} = \tilde{\mathbf{G}}(\tilde{\mathbf{G}} + \mathbf{R}^{-1})^{-1}\mathbf{R}^{-1}$. The division is illustrated in Fig. 2(c). Since the magnitude of graphene resistance in this division is largely arbitrary, the graphene resistance value is based on theoretical sheet conductivity at given gate voltage value. The resistances are listed in Table I.

It can be seen that the contacts 1–3 have comparable resistances far from the CNP while contact 4 has higher resistance. The differences between the contacts become more significant when approaching the CNP.

The relatively high contact resistances (R_i) are to a large extent explained by narrow regions in the graphene, which can be thought as graphene nanoconstrictions [35–37]. Therefore, their effect is briefly studied below. The conductance of such nanoconstriction is given by

$$G_{\mathrm{GNC}} = \frac{4e^2}{h}\frac{c_0 W k_{\mathrm{F}}}{\pi}, \tag{17}$$

where $c_0 (\leqslant 1)$ is related to edge roughness ($c_0 < 1$ for rough edges), W is the width of the constriction, and $k_{\mathrm{F}} = \sqrt{\pi n}$ is the Fermi wave vector in graphene. For a 300 nm gate oxide $n \approx |V_g - V_{g,\mathrm{CNP}}| \times 7.2 \times 10^{10}$ cm^{-2}, where $V_{g,\mathrm{CNP}}$ is the gate voltage corresponding to the charge neutrality point [38].

The blue curve in Fig. 2(d) shows the measured conductance as a function of gate voltage between terminals 1 and 3 (with 2 and 4 floating, i.e., $I_2 = I_4 = 0$) and fitted to the constriction model [Eq. (17)] as $G_1 = (R_1 + R_c + R_3)^{-1} = G_{\mathrm{GNC}}/4$, where the resistance of the central region, $R_c = (G_f + G_n)^{-1}$, contributes by 50% to the total resistance (far from the CNP) according to our conductance model. In the calculation we use $W = 50$ nm (estimated from a SEM image) and set the value of k_{F} to its theoretical value. Good agreement is found by setting the edge roughness parameter $c_0 \approx 0.90$, which is close to the previously reported experimental values 0.56 [35] and 0.74 [37]. One may also deduce the number of conduction channels in the contacts ($= W k_{\mathrm{F}}/\pi$), which becomes ~7 far from the CNP ($V_g = -10$ V) and ~3 near it ($V_g = +15$ V) in our device. However, it should be noted that the presence of increased carrier density due to proximity of metallic contacts can increase k_{F}, leading to smaller c_0, and therefore the obtained parameter values are only estimates. Also, here we assume $R_i = G_{\mathrm{GNC}}^{-1}$, ignoring possible other contributions to contact resistance. We note that the nonzero conductance near the CNP is most probably caused by doping from contacts and impurities.

C. Numerical calculations

We base our numerical calculations on the coherent and hot electron models described above. While the contact contributions are readily obtainable from the first terms of Eqs. (11) and (13), the graphene terms are calculated numerically. We find the four characteristic functions ϕ_k by numerically solving [39] the diffusion equation $\nabla \cdot \hat{\sigma} \nabla \phi_k = 0$ in a 2D geometry representing the graphene box. The chamfered corner terminals (width 20% of the box edge) have a constant voltage by setting $V_m = \delta_{mn} V_0$ (for ϕ_n) for the whole system, and subtracting the voltage drop in each contact, calculated using $\mathbf{G}$ and $\mathbf{R}$. Thus the corner terminals have the Dirichlet boundary condition while the box edges have zero perpendicular flux (Neumann boundary). The values of ϕ_k (for $k = \{2, 4\}$) and $\nabla\phi_k$ (for $k = \{1, 3\}$) are evaluated in a ~670 × 670 grid for numerical integration.

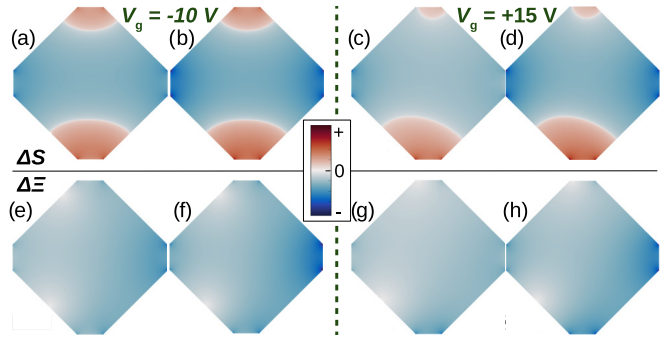

FIG. 3. Calculated integrands of ΔS (top row) and $\Delta\Xi$ probed at terminal 1 on the right [see Fig. 1(a) for terminal numbering] (bottom row) at $V_g = -10$ V (left half) and $V_g = +15$ V (right half) with coherent [(a), (c), (e), (g)] and hot electron models [(b), (d), (f), (h)]. The plots show cube roots of the data to enhance the visual clarity. All values are scaled with their respective integrated $S_A + S_B$ (or $\Xi_A + \Xi_B$) for comparison.

We obtain the noise cross-correlations S_{13} in bias configurations A, B, and C (denoted by $S_{A,B,C}$) and equivalently the autocorrelations S_{11} and S_{33}, which are denoted by $\Xi_{A,B,C}$. To compare the calculated and measured results more easily we introduce a dimensionless scaled exchange factor $\Delta S_{\mathrm{scaled}} = \Delta S/(S_A + S_B)$ (and similarly $\Delta\Xi_{\mathrm{scaled}}$). Both quantities are calculated far from the CNP (at $V_g = -10$ V) and near it (at $V_g = +15$ V, while $V_{g,\mathrm{CNP}} \approx +20$ V). The contact Fano factors turn out to have only little effect on the end result, and hence we set $F_i = 1/3$; equivalent results are obtained even with values approaching the quantum point contact limit ($F_i = 0$). Since the applied bias is relatively large, we can use the assumption $k_{\mathrm{B}}T_0 \ll eV$ in the hot electron regime.

The calculated distributions of the Π function in bias configuration A (and equivalent temperature T for hot electron regime) are presented in Figs. 1(b)–1(e). It can be seen that the distribution concentrates near the biasing terminal in the coherent regime [(b), (c)] while more uniform distributions are observed in the hot electron regime [(d), (e)]. The increased asymmetry of contact resistances near the CNP [(c), (e)] is also reflected to the noise distributions.

The distributions of the exchange factors ΔS and $\Delta\Xi$ are shown in Fig. 3. The integrated values of the these quantities are negative, although the distributions of ΔS have a positive contribution near the biasing contacts 2 and 4, where $\nabla\phi_1 \cdot \nabla\phi_3 < 0$. The low conductance of contact 4 reduces the size of the positive region near it, and increased conductance asymmetry at $V_g = +15$ V also clearly increases the asymmetry in the distributions. In general, the difference between the coherent and hot electron regimes appears as a small change in the overall level, although the integrated values show larger difference. The values of $\Delta\Xi$ are negative over the whole box, and the distributions are slightly concentrated toward the probing terminal 1 (on the right).

The calculated $\Delta S_{\mathrm{scaled}}$ and $\Delta\Xi_{\mathrm{scaled}}$ including the contact and graphene contributions in coherent and hot electron

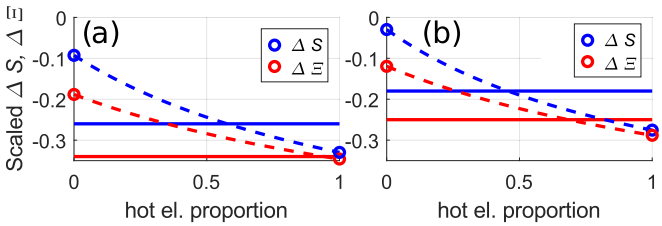

FIG. 4. Calculated scaled exchange factors ΔS_{scaled} (blue circles) and $\Delta \Xi_{\text{scaled}}$ (red circles) for coherent and hot electron models at (a) $V_g = -10$ V and (b) $V_g = +15$ V. The solid lines indicate approximate experimental results (see Fig. 7). The dashed curves connecting the two regimes are calculated from linearly interpolated $S_{A,B,C}$ and $\Xi_{A,B,C}$ between the coherent and hot electron values.

regimes are plotted in Figs. 4(a) and 4(b) for far and near the CNP, respectively. The exchange factors are plotted as a function of hot electron proportion: the coherent result is on the left end and the hot electron result on the right with a crossover regime between the two extremes. It can be seen that the coherent model results in too weak exchange factors compared to the experiment, while the hot electron regime produces too strong ΔS_{scaled}. Since the experimental results fall between the two regimes, we approximate the coherent–hot electron crossover regime by applying linear interpolation as a function of the hot electron contribution to calculated cross- and autocorrelations ($S_{A,B,C}$ and $\Xi_{A,B,C}$) individually and calculate the resulting exchange factors which are shown as dashed lines in Fig. 4. A relatively good agreement is obtained at ∼60% hot electron contribution at $V_g = -10$ V and ∼50% at $V_g = +15$ V. It should be noted, however, that such interpolation only provides a rough estimate of the behavior in the crossover regime.

III. EXPERIMENTAL METHODS

The sample [see Fig. 1(a)] is fabricated from micromechanically cleaved graphene on a heavily p-doped substrate with 300 nm gate oxide. The graphene extends under the Cr/Au contact electrodes. The bonding pads are sufficiently small ($150 \times 150\ \mu\text{m}^2$) so that only 10% of noise is shunted capacitively to the back-gate electrode.

A schematic of the experimental setup is shown in Fig. 5. The experiments are conducted on a BlueFors dry dilution refrigerator at 20 mK. The sample is connected to two high-frequency measurement channels with bias tees separating the DC and RF paths. Both channels have homemade HEMT low-noise amplifiers (LNA) mounted at the 4 K stage [40] reaching system noise temperatures of ∼10 K for channel

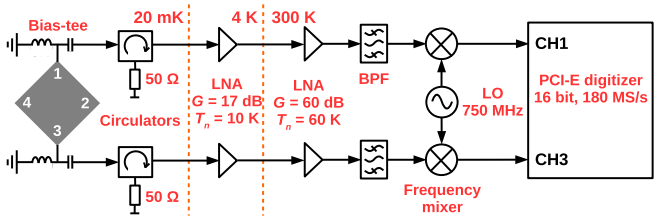

FIG. 5. Schematic of the measurement configuration.

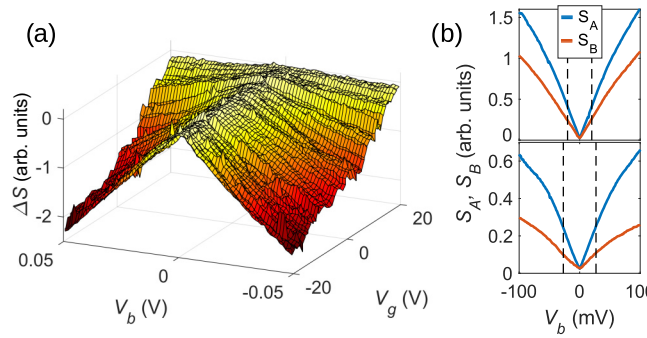

FIG. 6. (a) HBT exchange contribution $\Delta S = S_C - S_A - S_B$ measured on the bias vs gate voltage plane. The linear negative slope at small bias indicates an approximately constant HBT exchange effect $\Delta S/(S_A + S_B)$ as a function of V_b. (b) Measured noise cross-correlations S_A and S_B (in arbitrary units) at $V_g = -10$ V (top) and $V_g = +15$ V (bottom). The dashed vertical lines denote the ranges $V_b = -20 \ldots +20$ mV (for $V_g \leqslant 0$ V) and $V_b = -27 \ldots +27$ mV (for $V_g > 0$ V), which are used for linear fits.

1 and ∼15 K for channel 3. After additional amplification and band-pass filtering (BPF) at room temperature the RF signal is mixed down with a local oscillator (LO) at 750 MHz and digitized at 180 megasamples per second (MS/s) with an AlazarTech ATS9642 digitizer connected to PCI-E bus of a desktop computer. The cross- and autocorrelations are calculated from the digitized data using graphics processing unit (GPU) acceleration. Noise power coupling issues were treated along the lines given in Ref. [41].

IV. RESULTS

Our cross-correlation results for the HBT exchange term $\Delta S = S_C - S_A - S_B$ are displayed in Fig. 6(a) on the plane spanned by the gate (V_g) and bias (V_b) voltages; the Dirac point is located around $V_g = +20$ V. At small bias, we observe a clear negative HBT effect; as expected for fermionic diffusion, the ΔS signal grows linearly with the bias voltage V_b. A suppression of noise due to the interference of mutually incoherent electrons has been observed in an experiment with a ballistic electron beam splitter [5]. Our results demonstrate that this effect is also observable in mesoscopic diffusive conductors.

The value for scaled ΔS was calculated by making linear fits to the measured noise cross-correlation $S_{A,B,C}$ versus bias voltage at $V_b = -20 \ldots 0$ and $0 \ldots +20$ mV for $V_g \leqslant 0$ V. The lower conductance near the CNP increases the variance of the data, and therefore a wider range of V_b between ±27 mV is used for $V_g > 0$ V. The data are linear within those intervals, as shown in Fig. 6(b), although some deviation emerges when approaching the Dirac point due to lower conductance. The use of smaller intervals in fitting increased the variance of the resulting ΔS due to statistical errors, but the average values remained the same. Therefore, our fits can be considered as small-bias extrapolation to zero bias. We calculate the exchange factors for negative and positive V_b separately to see the scattering of the data.

The determined ΔS_{scaled} as a function of gate voltage is shown in Fig. 7(a) together with numerical results of the

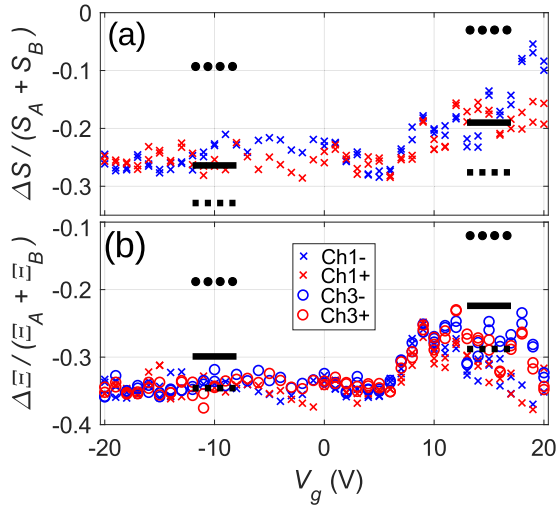

FIG. 7. (a) Scaled cross-correlation HBT exchange effect $\Delta S/(S_A + S_B)$ with blue (red) markers corresponding to negative (positive) V_b. The black lines dotted with circles and squares denote the results of diffusive calculation in coherent and hot electron regimes, respectively (see Fig. 4), while the solid black lines are interpolations in the crossover regime between coherent and hot electron regimes. (b) Scaled autocorrelation HBT exchange effect measured at terminals 1 and 3. For the linear interpolations, the hot electron contributions are taken as 60% for $V_g = -10$ V and 50% for $V_g = +15$ V.

coherent and hot electron models ($V_g \approx -10$ V) and close to ($V_g \approx +15$ V) the CNP. The data are scattered mainly due to statistical errors, although a clear trend in ΔS_{scaled} can be seen: the effect stays rather constant between -20 V $\leqslant V_g \lesssim +5$ V and tends linearly toward zero when approaching the Dirac point. The increased scattering of the data at large V_g is due to smaller absolute values of noise, as seen in Fig. 6, and the resulting statistical error.

In addition to cross-correlations, we determined the scaled exchange factors $\Delta\Xi_{\text{scaled}}$ for the measured noise in individual channels (autocorrelation). The obtained $\Delta\Xi_{\text{scaled}}$ are shown in Fig. 7(b) together with the results of the numerical model. $\Delta\Xi_{\text{scaled}}$ shows similar constant behavior below $V_g \approx +5$ V as ΔS_{scaled}, but the slope approaching the CNP is steeper and the scattering near CNP is significant.

When comparing the experimentally determined exchange factors to the results from diffusive calculations described in Sec. II C, it can be seen that the experimental values are situated between the coherent and hot electron results (black lines dashed with circles and squares, respectively, in Fig. 7). For autocorrelation, the experimental results agree well with the hot electron model, but for cross-correlation the hot electron model results in a too strong HBT exchange effect. For best overall agreement, we obtain linearly interpolated values in the crossover regime (see Fig. 4) with 60% hot electron contribution far from the CNP and 50% close the CNP. The interpolated values are shown as solid black lines in Fig. 7. As already mentioned, however, such linear interpolation gives an inadequate picture of the crossover regime, and therefore the interpolated values should only be considered as rough estimates.

V. DISCUSSION

There are several ways to construct a model for a graphene box. One of the simplest is the chaotic quantum dot described by a single distribution function [42]. A straightforward generalization of this model is to adopt the semiclassical model and to describe the graphene using a single distribution function governed by contact resistances with an arbitrary Fano factor. This model is in fact quite close to the model employed in Ref. [13]. Such a model, lacking voltage variation over the graphene box, was not able to match all the measured quantities G_{ij}, S_{11}, S_{33}, S_{13} properly. First after inclusion of the characteristic potential distributions, a satisfactory agreement could be achieved.

Closest to the present work is our previous experiment with a graphene cross sample with 50 nm nanoribbon arms [13]. In that graphene cross the HBT effect was characterized by occupation number noise in the nearly ballistic central region and regular diffusive noise in the ribbon arms. The HBT effect far from CNP in the cross sample ($\Delta S_{\text{scaled}} \approx -0.18$) is of comparable magnitude to that in the box (≈ -0.26), while the HBT effect near the CNP was strongly enhanced in the cross sample (to $\Delta S_{\text{scaled}} \approx -1.5$) but is suppressed in the graphene box. This is in line with the theoretical findings [11] that geometrical details of the sample strongly affect the observed HBT exchange effect.

The shot noise in our sample is generated in the central graphene region, as well as the narrow constrictions at the contacts contributing significantly to sample resistance [see Eq. (11)]. The contact resistances affect the characteristic potential distribution in the central region, and thus also their asymmetry has significant effect on the noise. We note that for such small contacts as we have in our sample, the contact capacitance can be regarded as negligible (on the basis of Ref. [43]), and the reactive impedance part at the noise measurement frequency does not bypass the contact resistance, resulting that the DC conductance values are sufficient for the noise circuit analysis.

The fact that the Dirac point in our sample is not well defined (see Figs. 2 and 7) indicates the presence of nonuniform doping, possibly due to contributions from fabrication residues, proximity of the contacts, and localized states at the edges. These locally varying doping effects would lead to nonuniform conductance in the regime of charge puddles near the Dirac point. Nonuniform conductance can easily be implemented in our numerical calculations, but this approach was not found exceedingly beneficial, and was given up due to further increase in the already high number of our fitting parameters. In addition, the characteristic statistics of the charge puddles are unknown, making it impossible to justify any specific configuration of nonuniformity in our model.

According to Fig. 7, our results are intermediate between coherent and hot electron transport. Theoretically, however, the strength of electron-electron interactions grows as V^2 due to the increase in the available scattering states with bias voltage. Therefore, we would expect the electron propagation in our graphene box to transform gradually with bias even closer to the hot electron regime with decreasing electron-electron scattering length $\ell_{\text{el-el}} < L$ [44]. Instead of an increase in the shot noise due to hot electron effects, we find a 5% decrease

in total F ($F = S_I/2eI$) at $V_b = 50$ mV compared with the value deduced using the low-bias Fano factor. This decrease is assigned to inelastic scattering, i.e., to the onset of scattering by polar surface modes in the graphene/SiO_2 system [45,46]. Our experimental results do not show any noticeable change in ΔS_{scaled} up to bias voltage $V_b = 50$ mV, and hence the pure hot electron regime was not fully achieved in our experiments. The independence of our results on bias at $|V_b| \lesssim 50$ mV suggests that ΔS and $\Delta\Xi$ might include features inherent to diffusive graphene.

It is instructive to consider the analogy between our experiment and interference experiments in optics. We note that in Eq. (7) the function Π is multiplied by gradients $\nabla\phi_m$ and $\nabla\phi_n$. In analogy with optics, these gradients can be interpreted as distributed detector functions "filtering" the Π function. They vary smoothly inside the graphene box, which implies that the whole box acts as an "interferometer screen." In this interpretation the noise cross-correlation is given by an area integral weighted with the geometric response functions. For a simple description, we employ an analogy with a double-slit experiment where the incoming intensity I on the detector is determined in three different configurations: the experiment is performed by closing first one slit (I_A), then the other slit (I_B), and finally by keeping both slits open (I_C); here the applied electric potential is the analog of light in the double-slit experiment. In our case, the "detection screen" is the whole graphene box where interference due to $f(1-f)$ takes place at every point. The recorded interference value is an integral provided by the cross-correlation measurements [see Eq. (7)] where we take the equivalent of $\Delta I = I_C - I_A - I_B$ (the difference between the actual interference pattern and the two backgrounds), namely $\Delta S = S_C - S_A - S_B$. Although this analog is illuminating for understanding the setting of our experiment, the underlying effects are two-particle interferences. The correlation effects arise via the competition of the available states in the reservoirs for the outgoing electrons. The nonequilibrium Π function [see Figs. 1(b) and 1(c)] carries this information over to the whole sample. However, the actual phase dependence of the two-particle scattering events is averaged out in our diffusive conductor [11]. Due to the lack of phase dependence, we prefer to call our observed results as HBT exchange effects, even though interference by two diffusive wave fronts describes the phenomena in the sense of our analogy.

VI. CONCLUSIONS

We have studied exchange cross-correlations in a disordered graphene box. Our experimental results display distinct Hanbury Brown and Twiss (HBT) exchange correlations, which deviate from the standard predictions of scattering matrix theory. Our results indicate that the finite contact resistances significantly affect the noise cross-correlations in a diffusive system. The values of experimentally determined HBT exchange effects fall between calculated values for coherent and hot electron models, indicating either the presence of a bias-independent crossover regime or intrinsic behavior of diffusive graphene which is not captured by the standard model for diffusive systems. The overall picture is the same for both near and far from the Dirac point, although the low carrier density near the CNP leads to further deviations between the model and experimental data.

ACKNOWLEDGMENTS

We thank Florian Libisch and Stefan Rotter for fruitful discussions. This work was supported by the Academy of Finland, Projects No. 314448 (BOLOSE), No. 310086 (LT-noise), No. 312295 (CoE, Quantum Technology Finland), and No. 312057 (Centre of Excellence program), as well as by ERC (Grant No. 670743). This research project utilized the Aalto University OtaNano/LTL infrastructure, which is part of the European Microkelvin Platform. T.E. is grateful to the Vilho, Yrjö, and Kalle Väisälä Foundation for support from a scholarship. The work of G.B.L. was supported by an Aalto University School of Science Visiting Professor grant, the Government of the Russian Federation (Agreement No. 05.Y09.21.0018), RFBR Grant No. 17-02-00396A, and the Foundation for the Advancement of Theoretical Physics and Mathematics "BASIS."

[1] S. Kogan, *Electronic Noise and Fluctuations in Solids* (Cambridge University Press, Cambridge, 1996).

[2] Y. M. Blanter and M. Büttiker, Shot noise in mesoscopic conductors, Phys. Rep. **336**, 1 (2000).

[3] T. Martin, Noise in mesoscopic physics, in *Les Houches Summer School Proceedings*, Vol. 81, edited by H. Bouchiat, Y. Gefen, S. Guéron, G. Montambaux, and J. Dalibard (Elsevier, Amsterdam, The Netherlands, 2005), Chap. 5, pp. 283–359.

[4] G. B. Lesovik and I. A. Sadovskyy, Scattering matrix approach to the description of quantum electron transport, Phys. Usp. **54**, 1007 (2011).

[5] R. C. Liu, B. Odom, Y. Yamamoto, and S. Tarucha, Quantum interference in electron collision, Nature (London) **391**, 263 (1998).

[6] W. D. Oliver, Hanbury Brown and Twiss–type experiment with electrons, Science **284**, 299 (1999).

[7] M. Henny, S. Oberholzer, C. Strunk, T. Heinzel, K. Ensslin, M. Holland, and C. Schönenberger, The fermionic Hanbury Brown and Twiss experiment, Science **284**, 296 (1999).

[8] D. C. Glattli, Tunneling experiments in the fractional quantum Hall effect regime, in *Quantum Hall Effect: Poincaré Seminar 2004*, edited by B. Douçot, V. Pasquier, B. Duplantier, and V. Rivasseau (Birkhäuser, Basel, 2005), pp. 163–197.

[9] R. Hanbury Brown and R. Q. Twiss, Correlation between photons in two coherent beams of light, Nature (London) **177**, 27 (1956).

[10] I. Neder, N. Ofek, Y. Chung, M. Heiblum, D. Mahalu, and V. Umansky, Interference between two indistinguishable electrons from independent sources, Nature (London) **448**, 333 (2007).

[11] Y. M. Blanter and M. Büttiker, Shot-noise current-current correlations in multiterminal diffusive conductors, Phys. Rev. B **56**, 2127 (1997).

[12] E. V. Sukhorukov and D. Loss, Noise in multiterminal diffusive conductors: Universality, nonlocality, and exchange effects, Phys. Rev. B **59**, 13054 (1999).
[13] Z. B. Tan, T. Elo, A. Puska, J. Sarkar, P. Lähteenmäki, F. Duerr, C. Gould, L. W. Molenkamp, K. E. Nagaev, and P. J. Hakonen, Hanbury-Brown and Twiss exchange and non-equilibrium-induced correlations in disordered, four-terminal graphene-ribbon conductor, Sci. Rep. **8**, 14952 (2018).
[14] M. I. Katsnelson, Zitterbewegung, chirality, and minimal conductivity in graphene, Eur. Phys. J. B **51**, 157 (2006).
[15] J. Tworzydło, B. Trauzettel, M. Titov, A. Rycerz, and C. W. J. Beenakker, Sub-Poissonian Shot Noise in Graphene, Phys. Rev. Lett. **96**, 246802 (2006).
[16] P. San-Jose, E. Prada, and D. S. Golubev, Universal scaling of current fluctuations in disordered graphene, Phys. Rev. B **76**, 195445 (2007).
[17] C. H. Lewenkopf, E. R. Mucciolo, and A. H. Castro Neto, Numerical studies of conductivity and Fano factor in disordered graphene, Phys. Rev. B **77**, 081410(R) (2008).
[18] M. A. Laakso and T. T. Heikkilä, Charge transport in ballistic multiprobe graphene structures, Phys. Rev. B **78**, 205420 (2008).
[19] L. DiCarlo, J. R. Williams, Y. Zhang, D. T. McClure, and C. M. Marcus, Shot Noise in Graphene, Phys. Rev. Lett. **100**, 156801 (2008).
[20] R. Danneau, F. Wu, M. F. Craciun, S. Russo, M. Y. Tomi, J. Salmilehto, A. F. Morpurgo, and P. J. Hakonen, Shot Noise in Ballistic Graphene, Phys. Rev. Lett. **100**, 196802 (2008).
[21] R. Danneau, F. Wu, M. F. Craciun, S. Russo, M. Y. Tomi, J. Salmilehto, A. F. Morpurgo, and P. J. Hakonen, Shot noise measurements in graphene, Solid State Commun. **149**, 1050 (2009).
[22] R. Danneau, F. Wu, M. Y. Tomi, J. B. Oostinga, A. F. Morpurgo, and P. J. Hakonen, Shot noise suppression and hopping conduction in graphene nanoribbons, Phys. Rev. B **82**, 161405(R) (2010).
[23] W. Schottky, Über spontane Stromschwankungen in verschiedenen Elektrizitätsleitern, Ann. Phys. **362**, 541 (1918).
[24] V. A. Khlus, Current and voltage fluctuations in microjunctions between normal metals and superconductors, Sov. Phys. JETP **66**, 1243 (1987).
[25] R. Landauer, Johnson-Nyquist noise derived from quantum mechanical transmission, Phys. D **38**, 226 (1989).
[26] G. B. Lesovik, Excess quantum noise in 2D ballistic point contacts, JETP Lett. **49**, 592 (1989).
[27] B. Yurke and G. P. Kochanski, Momentum noise in vacuum tunneling transducers, Phys. Rev. B **41**, 8184 (1990).
[28] M. Büttiker, Scattering Theory of Thermal and Excess Noise in Open Conductors, Phys. Rev. Lett. **65**, 2901 (1990).
[29] C. W. J. Beenakker and M. Büttiker, Suppression of shot noise in metallic diffusive conductors, Phys. Rev. B **46**, 1889 (1992).
[30] K. Nagaev, On the shot noise in dirty metal contacts, Phys. Lett. A **169**, 103 (1992).
[31] D. S. Fisher and P. A. Lee, Relation between conductivity and transmission matrix, Phys. Rev. B **23**, 6851 (1981).
[32] I. Aleiner, P. Brouwer, and L. Glazman, Quantum effects in Coulomb blockade, Phys. Rep. **358**, 309 (2002).
[33] E. V. Sukhorukov and D. Loss, Universality of Shot Noise in Multiterminal Diffusive Conductors, Phys. Rev. Lett. **80**, 4959 (1998).
[34] J. Voutilainen, A. Fay, P. Häkkinen, J. K. Viljas, T. T. Heikkilä, and P. J. Hakonen, Energy relaxation in graphene and its measurement with supercurrent, Phys. Rev. B **84**, 045419 (2011).
[35] B. Terrés, L. A. Chizhova, F. Libisch, J. Peiro, D. Jörger, S. Engels, A. Girschik, K. Watanabe, T. Taniguchi, S. V. Rotkin, J. Burgdörfer, and C. Stampfer, Size quantization of Dirac fermions in graphene constrictions, Nat. Commun. **7**, 11528 (2016).
[36] R. Krishna Kumar, D. A. Bandurin, F. M. Pellegrino, Y. Cao, A. Principi, H. Guo, G. H. Auton, M. Ben Shalom, L. A. Ponomarenko, G. Falkovich, K. Watanabe, T. Taniguchi, I. V. Grigorieva, L. S. Levitov, M. Polini, and A. K. Geim, Superballistic flow of viscous electron fluid through graphene constrictions, Nat. Phys. **13**, 1182 (2017).
[37] V. Clericò, J. A. Delgado-Notario, M. Saiz-Bretín, C. Hernández Fuentevilla, A. V. Malyshev, J. D. Lejarreta, E. Diez, and F. Domínguez-Adame, Quantized Electron Transport through Graphene Nanoconstrictions, Phys. Status Solidi **215**, 1701065 (2018).
[38] S. Das Sarma, S. Adam, E. H. Hwang, and E. Rossi, Electronic transport in two-dimensional graphene, Rev. Mod. Phys. **83**, 407 (2011).
[39] COMSOL MULTIPHYSICS was used for the calculation.
[40] T. Nieminen, P. Lähteenmäki, Z. Tan, D. Cox, and P. J. Hakonen, Low-noise correlation measurements based on software-defined-radio receivers and cooled microwave amplifiers, Rev. Sci. Instrum. **87**, 114706 (2016).
[41] R. Danneau, F. Wu, M. F. Craciun, S. Russo, M. Y. Tomi, J. Salmilehto, A. F. Morpurgo, and P. J. Hakonen, Evanescent wave transport and shot noise in graphene: Ballistic regime and effect of disorder, J. Low Temp. Phys. **153**, 374 (2008).
[42] S. A. van Langen and M. Büttiker, Quantum-statistical current correlations in multilead chaotic cavities, Phys. Rev. B **56**, R1680 (1997).
[43] A. Laitinen, G. S. Paraoanu, M. Oksanen, M. F. Craciun, S. Russo, E. Sonin, and P. Hakonen, Contact doping, Klein tunneling, and asymmetry of shot noise in suspended graphene, Phys. Rev. B **93**, 115413 (2016).
[44] K. E. Nagaev, Influence of electron-electron scattering on shot noise in diffusive contacts, Phys. Rev. B **52**, 4740 (1995).
[45] J.-H. Chen, C. Jang, S. Xiao, M. Ishigami, and M. S. Fuhrer, Intrinsic and extrinsic performance limits of graphene devices on SiO_2, Nat. Nanotechnol. **3**, 206 (2008).
[46] S. Fratini and F. Guinea, Substrate-limited electron dynamics in graphene, Phys. Rev. B **77**, 195415 (2008).